



Cite this: *RSC Adv.*, 2021, 11, 22805

# Green sonochemistry assisted synthesis of hollow magnetic and photoluminescent $\text{MgFe}_2\text{O}_4$ –carbon dot nanocomposite as a sensor for toxic $\text{Ni(II)}$ , $\text{Cd(II)}$ and $\text{Hg(II)}$ ions and bacteria

Shahla Ahmadian-Fard-Fini,<sup>a</sup> Davood Ghanbari,<sup>\*b</sup> Omid Amiri<sup>cd</sup> and Masoud Salavati-Niasari <sup>\*a</sup>

The purpose of this study was synthesis of photoluminescent nanoparticles for detection of toxic metal ions. Also, these controllable magnetic nanocomposites were used for detection of *Pseudomonas aeruginosa* bacteria. Carbon nano-templates were formed by calcination and sonication of lemon extract as a bio-compatible precursor. Then  $\text{MgFe}_2\text{O}_4$  nanoparticles were incorporated on the carbon nano-templates. The composite was calcinated to decompose carbon and obtain hollow structures. Finally, photoluminescent carbon dots were deposited on the porous magnesium ferrite core. Because of the hollow structure, carbon dots can diffuse to the Mg-ferrite core so magnetic and photoluminescence properties are available simultaneously. Photoluminescence intensity decreases with increasing  $\text{Ni(II)}$ ,  $\text{Cd(II)}$ ,  $\text{Hg(II)}$  metal ions and *Pseudomonas aeruginosa*. Results show an effective nanostructure for identification of toxic metal ions and also bacteria.

Received 28th March 2021

Accepted 15th June 2021

DOI: 10.1039/d1ra02458b

rsc.li/rsc-advances

## 1. Introduction

Carbon dots (CDs) originating from graphene have both  $\text{sp}^3$  and  $\text{sp}^2$  hybridization (with carbon–oxygen or hydrogen–oxygen functional groups). Relative to typical quantum dots, CDs are desirable substitutes considering their chemical durability and lack of harmful components.<sup>1,2</sup> The main properties of CDs are easy electron transportation, low price, controllable photoluminescence (PL), multi-photon stimulation, broad range light emission, easy functionalization, dispersibility in polar solvents, and stability against photo-bleaching and photo-blinking. Luminescence may originate from defects and traps, quantum-confinement of excitons, and also ring structures.<sup>3–6</sup> Green fluorescence can be used as a sensor in cell imaging and other biomedical applications.<sup>7–12</sup>

Sono-chemistry at frequencies higher than 20 kHz has many applications in, for example, structural analysis, determination of distance, sono-photographic healing, removing dirt, and transfer of information. When sound waves with frequencies higher than 20 000 MHz in a liquid, they can break chemical bonds (sonolysis) and produce free radicals. In sono-chemistry,

nucleation, cavitation, bubble interactions and effective chemical processes occur. Sono-chemistry is helpful in enhancing the rate of catalytic reactions, increasing degradation of pollutants (like pharmaceutical waste), and preparation of new materials.<sup>13–15</sup> Ultrasonication leads to high pressure in liquids (compression); increase in pressure causes bubbles to become smaller, and lowering of pressure leads to expansion of bubbles. Bubbles become larger in a widespread way, with cycles until the ultrasound energy can no more be captured and the forces lead to strong breakdown. In water as solvent, reduction–oxidation reactions occur and hydrogen and hydroxyl radicals are produced.<sup>16–18</sup>

A lot of industrial and urban pollutants have been covertly added to pure water sources, one of the main group of toxic pollutants being heavy metal ions, which can have harmful effects on biological systems. As we know, these toxic ions can cause various mutations in biological systems, so portable and easy detection of them is necessary for protecting community health. Bio-compatible magnetic materials like magnetite have attracted much attention for use as a core for accommodating nanostructures; in this work another biocompatible material, magnesium ferrite, was selected based on its reported appropriate properties.<sup>19,20</sup>

Commonly, bacterial testing requires time and pricey instruments for identification, which is not acceptable in disease emergency conditions, so rapid recognition of bacteria is important for prevention of contagion. *Pseudomonas aeruginosa* is resistant to antibiotics; this bacterium can develop in

<sup>a</sup>Institute of Nano Science and Nano Technology, University of Kashan, P. O. Box 87317-51167, Kashan, Iran. E-mail: salavati@kashanu.ac.ir

<sup>b</sup>Department of Science, Arak University of Technology, Arak, Iran. E-mail: d-ghanbari@arakut.ac.ir

<sup>c</sup>Faculty of Chemistry, Razi University, Kermanshah, 6714414971, Iran

<sup>d</sup>Department of Chemistry, College of Science, University of Raparin, Rania, Kurdistan Region, Iraq


low-oxygen atmospheres, it can cause disease in people, and it is known to appear in every part of the body, notably in healing wounds. If essential organs are colonized, infection can even be fatal.<sup>21–23</sup> In this work, fluorescent hollow magnesium ferrite-CDs were prepared for rapid identification of bacteria, using sono-chemical and hydrothermal treatment.

## 2. Experimental

### 2.1. Synthesis of carbon dots

Ethylene diamine (0.6 g, 0.01 mol) and citric acid monohydrate (2.1 g, 0.01 mol) were dissolved in 500 ml of water. Next, the solution was autoclaved (Teflon-lined stainless steel) at 200 °C for 24 h. The final product was dispersed in water using ultra-sonic radiation (100–150 W, 30–60 min).

### 2.2. Synthesis of $\text{MgFe}_2\text{O}_4$ nanostructures

Carbon (as template for giving a particular shape) was obtained by calcination (350 °C, 2 h) of lemon extract. To eliminate agglomeration the product was dispersed in water under sonication (150 W, 1 h). Next, 0.2 g of the carbon, 0.02 mol of  $\text{Mg}(\text{NO}_3)_2 \cdot 6\text{H}_2\text{O}$  and 0.04 mol of iron nitrate  $\cdot 9\text{H}_2\text{O}$  were added to water (200 ml). Sodium hydroxide solution (1 M, 15 ml) was added to adjust the pH to 11. After that the reaction mixture was autoclaved at 200 °C for 12 h; then the gray product was

collected and washed with de-ionized water and ethanol. Finally, the compound was calcinated at 600 °C for 3 h for carbon decomposition. 0.2 g of magnesium ferrite was dispersed in 50 ml of water. Also, for suitable dispersion and to prevent agglomeration, ultra-sonic waves were applied (100–150 W, 30–60 min).

### 2.3. $\text{MgFe}_2\text{O}_4$ -carbon dot nanostructures

Magnesium ferrite (0.2 g) was dispersed in 50 ml of de-ionized water and then both citric acid and ethylene diamine (0.02 mol) were dissolved and the solution was autoclaved (Teflon-lined stainless steel) at 200 °C for 24 h; it was then centrifuged and the solid product was washed with ethanol.

## 3. Results and discussion

A schematic of the synthesis of  $\text{MgFe}_2\text{O}_4$ -carbon dots by the solvo-thermal method is depicted in Fig. 1. Brunauer–Emmett–Teller (BET) results for the prepared carbon dots are shown in Table 1. Fig. 2a shows the X-ray diffraction spectrum of carbon

Table 1 BET results of carbon dots

BET plot		
$V_m$	7.64	$[\text{cm}^3(\text{STP}) \text{ g}^{-1}]$
$a_{s,\text{BET}}$	33.35	$[\text{m}^2 \text{ g}^{-1}]$
$C$	151.07	
Total pore volume ( $p/p_0 = 0.990$ )	0.944	$[\text{cm}^3 \text{ g}^{-1}]$
Average pore diameter	9.39	$[\text{nm}]$

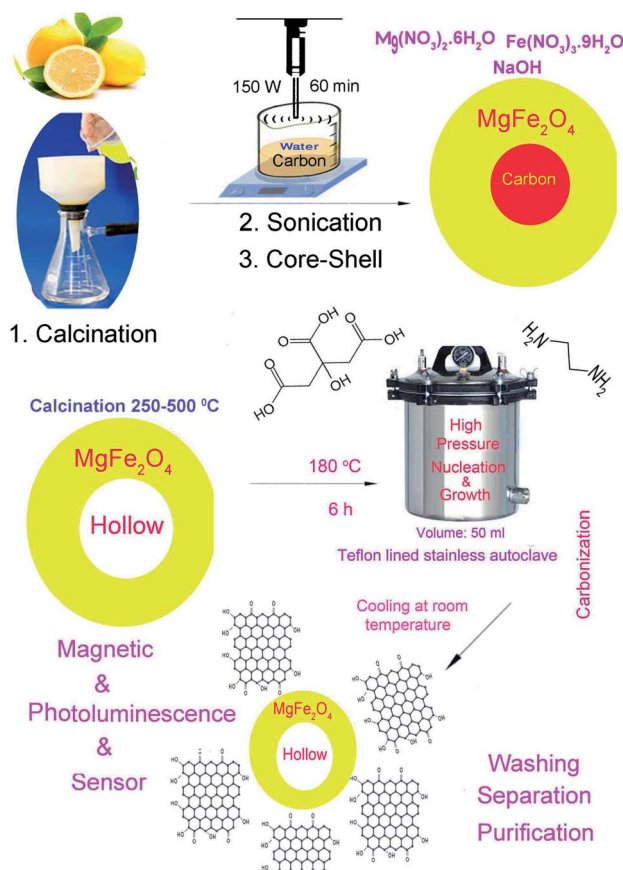


Fig. 1 Schematic of preparation of carbon dots and hollow magnetic nanocomposite.

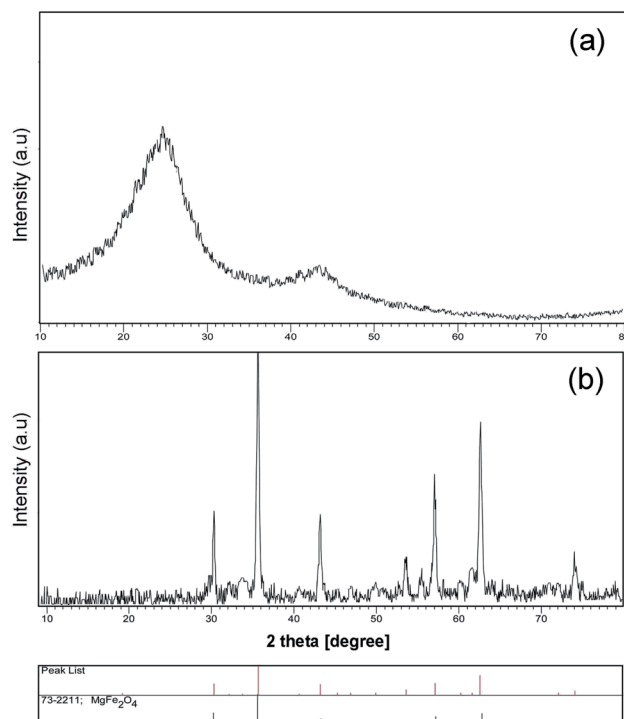


Fig. 2 XRD patterns of (a) carbon dot nanoparticles, and (b)  $\text{MgFe}_2\text{O}_4$ -carbon dot nanocomposite.



dots obtained at 200 °C for 6 h, which is in agreement with the literature, and shows an amorphous semi-crystalline pattern.<sup>1,3,4</sup> Fig. 2b displays the X-ray diffraction (XRD) pattern of the magnesium ferrite-carbon dot product. The inverse spinel (phase: cubic) structure of  $\text{MgFe}_2\text{O}_4$  (73-2211 JCPDS number, number 227 of  $Fd\bar{3}m$  space group) was confirmed.

The luminescence of the CDs samples was investigated using ultra-violet irradiation. Samples are yellow under ambient light; however, they are green under UV exposure.

Fig. 3a displays a scanning electron microscopy (SEM) image of the carbon template obtained from lemon extract calcination (green precursor), which confirms preparation of tetragonal structures; according to the images obtained, the average diameter is about 200 nm. High temperature leads to agglomeration and aggregation, so in this work ultrasound radiation was also used to prepare mono-disperse nanoparticles. Three locations for reaction exist in sono-chemistry: the gas in the bubbles (pyrolysis), the surface of bubbles (reactions happen in  $P$ - $T$  gradients) and the mass solution (energy is transferred to the solvent and multiplies the bubbles). Temperature, pressure, frequency, vessel shape, transducer, and addition of liquid and

gas can affect the final product in the sono-chemical reactor.<sup>13,16,17</sup>

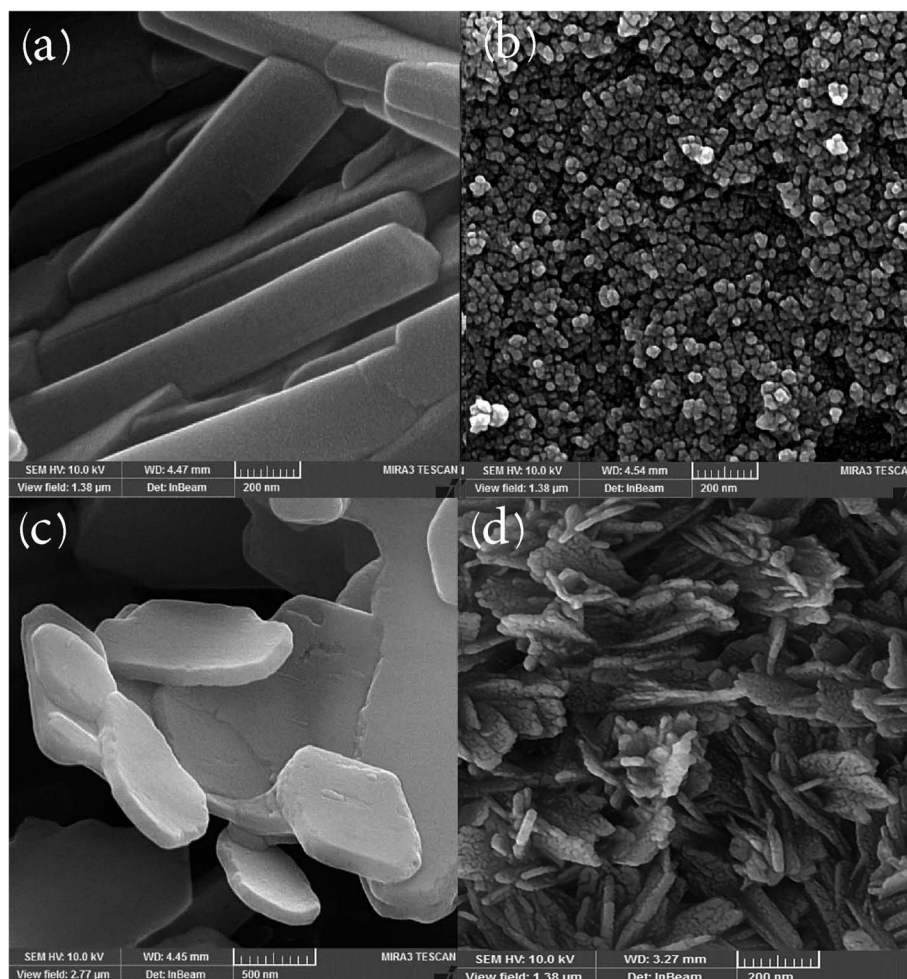
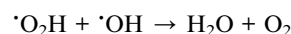
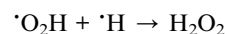
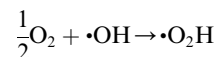
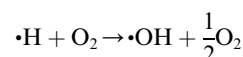
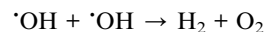
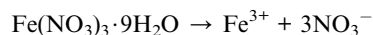
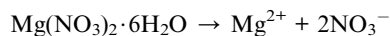


Fig. 3 SEM images of (a) tetragonal carbon template prepared by calcination and (b) by sono-chemical method; (c) hexagonal  $\text{MgFe}_2\text{O}_4$  prepared by hydrothermal method; (d)  $\text{MgFe}_2\text{O}_4$  nanoparticles after calcination and sonication.

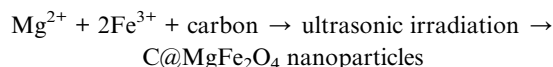




$\text{C}_6\text{H}_8\text{O}_7$  (lemon extract : citric acid)  $\rightarrow$  thermal decomposition  $\rightarrow$  carbon nanoplates



Carbon nanoplates  $\rightarrow$  ultrasonic irradiation  $\rightarrow$  carbon nanoparticles



C@MgFe<sub>2</sub>O<sub>4</sub> nanoparticles  $\rightarrow$  calcination  $\rightarrow$  hollow MgFe<sub>2</sub>O<sub>4</sub>

Hollow MgFe<sub>2</sub>O<sub>4</sub> + carbon dot  $\rightarrow$  ultrasonic irradiation  $\rightarrow$  hollow MgFe<sub>2</sub>O<sub>4</sub>@carbon dot

By breakdown of bubbles that are created in solvent, micro-jets can break bonds and decrease accumulation.

Fig. 3b depicts a SEM image of carbon nanoparticles prepared under ultrasonic irradiation (150 W for 1 h), which confirms the presence of approximately mono-disperse nanostructures and shows their average size is around 60 nm.

Fig. 3c exhibits a SEM image of MgFe<sub>2</sub>O<sub>4</sub> synthesized by the hydrothermal method. As we expected, MgFe<sub>2</sub>O<sub>4</sub> has

a hexagonal structure, and interestingly it is observed that micro-hexagons were synthesized. Our results prove precipitation is not effective for breaking of magnetic domains in this structure, so we applied higher temperature for removing of further materials, and outcomes show that by applying hydro-thermal and sono-chemical methods, micro-structures are converted to nanostructures. Fig. 3d depicts a SEM image of MgFe<sub>2</sub>O<sub>4</sub> after calcination (500 °C, 2 h) and sonication (150 W for 1 h). As particle size analysis verifies, the average size of the nanostructures is lower than 50 nm. With explosion in the bubbles, smaller compounds are obtained in hot small reactors. Our results confirm that by applying ultrasonic irradiation, tetragonal micro-structures are broken down and converted to semi-spherical nanoparticles with average diameter around 40 nm. For better dispersion, ultrasonic irradiation was performed after the solvo-thermal process. By increasing the temperature and accordingly the pressure in a closed reactor, carbon dots were appropriately synthesized, with an average size of about 30 nm.

Fig. 4 illustrates transmission electron microscopy (TEM) images of magnesium ferrite-carbon dots. Interestingly, TEM images confirm magnesium ferrite is covered with carbon dots and a two-phase nanocomposite has been synthesized; high resolution TEM images show that the distance between crystal planes is about 2.5 Å, in agreement with XRD of pure standards.

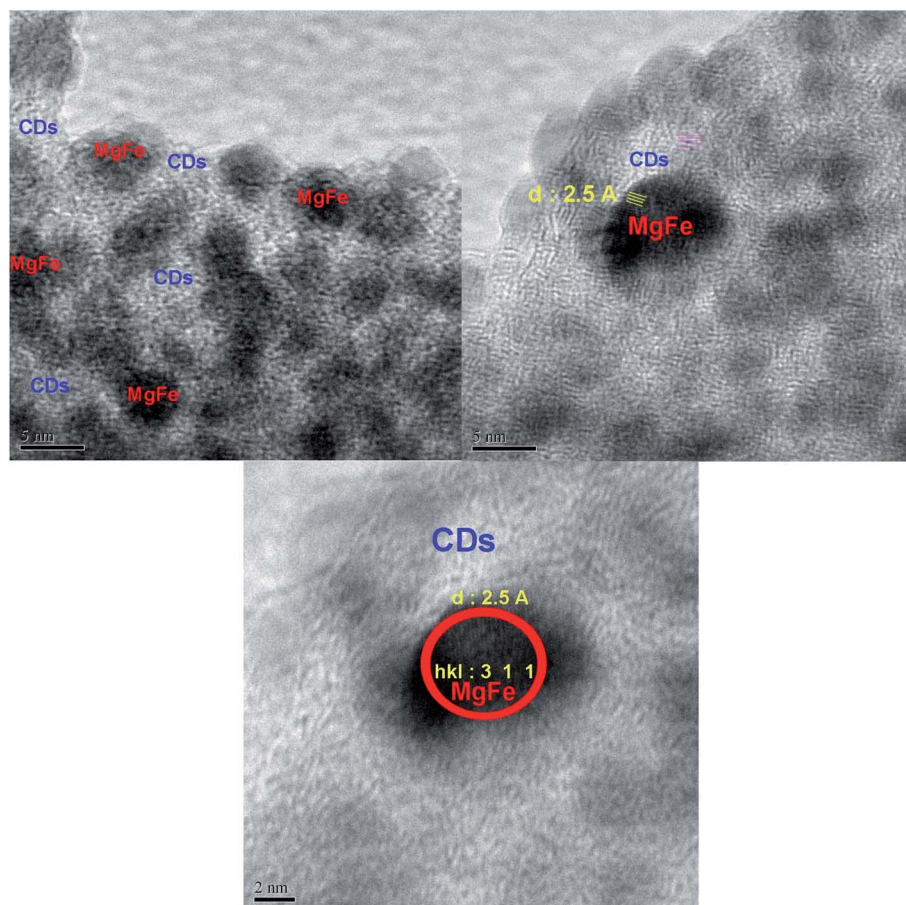


Fig. 4 TEM images of MgFe<sub>2</sub>O<sub>4</sub>-carbon dot nanocomposite.



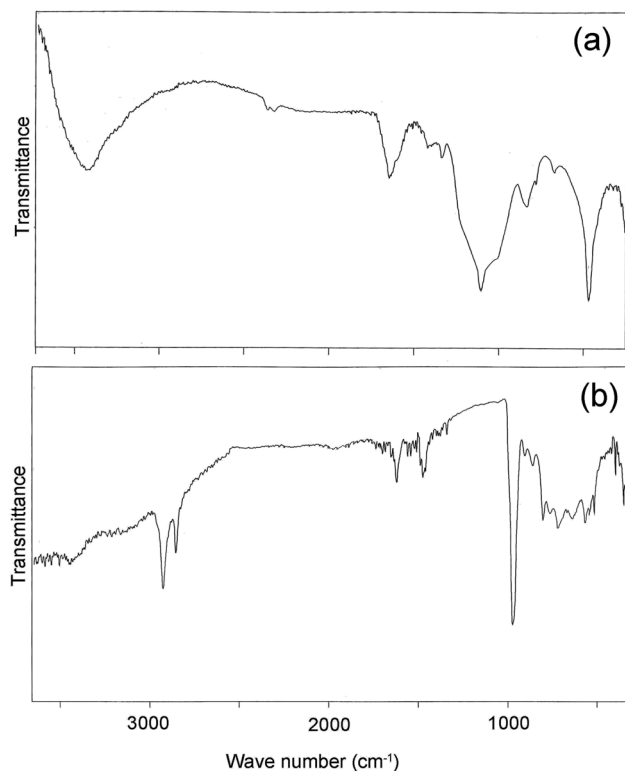


Fig. 5 FT-IR curves of (a)  $\text{MgFe}_2\text{O}_4$  nanoparticles, and (b)  $\text{MgFe}_2\text{O}_4$ -carbon nanocomposite.

The images verify that the size of these porous nanostructures is less than 10 nm.

Fig. 5a depicts Fourier transform infra-red spectra of the magnesium ferrite; the peak at  $470\text{ cm}^{-1}$  is for Mg-O and Fe-O bonds, and the wide absorption at  $3416\text{ cm}^{-1}$  is due to the O-H bond. The peak at  $1103\text{ cm}^{-1}$  results from C-O bonds in citric acid. Fig. 5b illustrates the spectrum of the  $\text{MgFe}_2\text{O}_4$ -CDs nanocomposite; the presence of carboxyl and hydroxyl functional groups is demonstrated in this spectrum. The absorption at  $972\text{ cm}^{-1}$  is attributed to C-O, and the bands at  $2850$  and  $2920\text{ cm}^{-1}$  are for C-H bonds; the signal at  $1620\text{ cm}^{-1}$  is due to C=O.

According to thermal gravimetric analysis (TGA), at temperatures of about  $100\text{--}140\text{ }^\circ\text{C}$  there is a small weight loss of around 5% due to hydroxyl groups and moisture on the hydrophilic structure, and there is also another obvious decrease of about 25% in the  $350\text{--}420\text{ }^\circ\text{C}$  range because of decomposition of the carbon dot coating; then from  $400$  to  $800\text{ }^\circ\text{C}$  the residual is constant owing to the thermal stability of the ferrite (metal-oxide).

A vibrating-sample magnetometer (VSM) was utilized to investigate magnetic properties; hysteresis loops for  $\text{MgFe}_2\text{O}_4$  and  $\text{MgFe}_2\text{O}_4$ -carbon nano-compounds can be seen in Fig. 6a and b respectively. The nano-compounds display appropriate magnetic induction rendering them adequate for detection uses. The curves exhibit ferromagnetic behavior, with  $22\text{ emu/g}$  saturation magnetization and  $70\text{ Oe}$  coercivity for  $\text{MgFe}_2\text{O}_4$ , and  $15\text{ emu/g}$  saturation magnetization and  $100\text{ Oe}$  coercivity for the  $\text{MgFe}_2\text{O}_4$ -carbon nano-compound.

Covering magnesium ferrite with carbon dots increased the coercivity from  $70\text{ Oe}$  to  $100\text{ Oe}$ . Domains are stuck together in

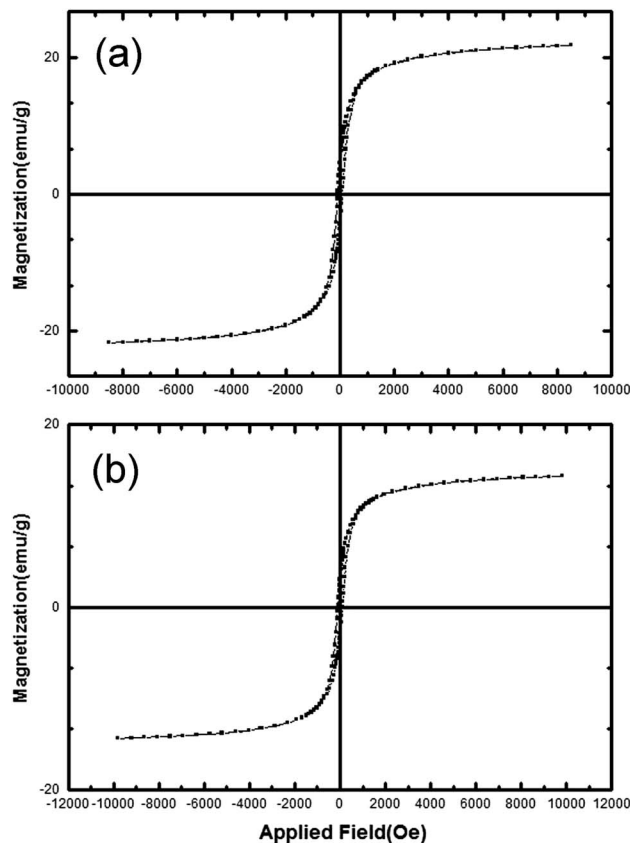


Fig. 6 VSM curves of (a)  $\text{MgFe}_2\text{O}_4$  nanoparticles, and (b)  $\text{MgFe}_2\text{O}_4$ -carbon dot nanocomposite.

the process and so stronger magnetic field is needed to change their directions.

The ultraviolet-visible (UV-Vis) absorption spectrum of the carbon dot nanocomposite prepared by the hydrothermal route at  $200\text{ }^\circ\text{C}$  is depicted in Fig. 7a. The compound displays an absorption peak at  $380\text{ nm}$  ( $\pi\text{--}\pi^*$  transition). CDs illustrate and achieve bandgap in comparison with conductive graphite due to quantum limitation, giving rise to UV absorption and PL peaks. Fig. 7b-d illustrate the Tyndall effect of the product in aqueous solution at different green, red and violet wavelengths. Beam scattering occurs when particles with approximately nano-dimensions are present in a solvent (colloid or nano-suspension). De-ionized water is shown beside the nanocomposite solutions for comparison. Electromagnetic radiation that has longer wavelength displays more transmission while shorter wavelengths exhibit more reflection.

Luminescence spectra of carbon dots synthesized at  $200\text{ }^\circ\text{C}$  and reacted with *Pseudomonas aeruginosa* are displayed in Fig. 8; the excitation wavelength was about  $450\text{ nm}$  and a PL peak at approximately  $580\text{ nm}$  was obtained. The results verify a decrease in luminescence with increase in quantity of *Pseudomonas aeruginosa* (quantum yield around 18%).<sup>1</sup> The surface electronic properties of the carbon nanostructure are changed by interaction with bacteria, extinguishing PL, which allows the concentration of the bacteria to be calculated.<sup>1</sup> PL spectra of untreated carbon dots and carbon dots reacted with nickel(II),

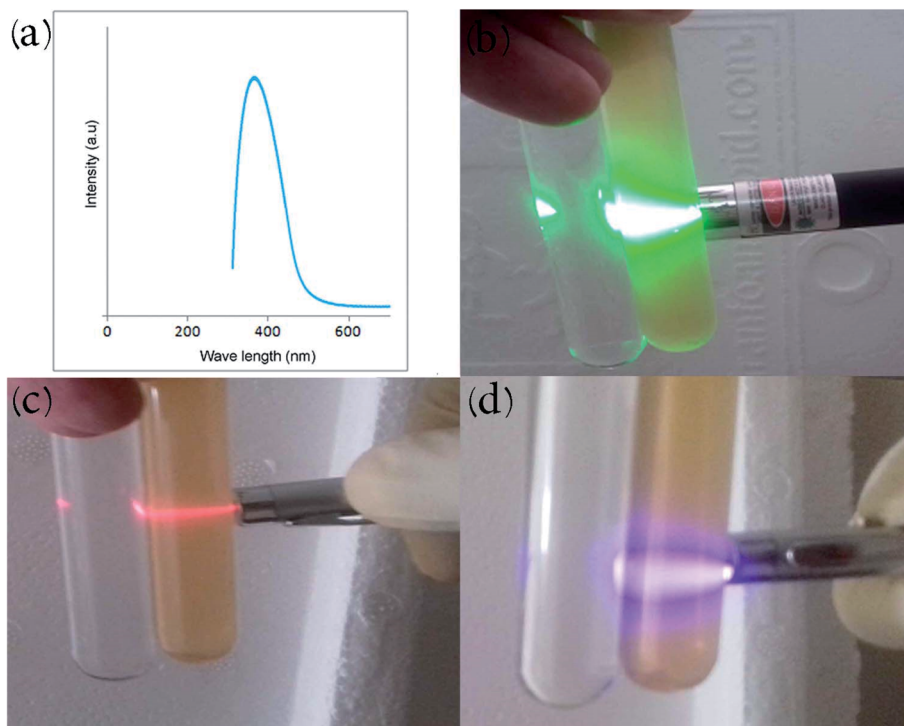


Fig. 7 (a) UV-Vis spectrum of the carbon dot nanocomposite. Tyndall effect of carbon dots in water with (b) green, (c) red and (d) violet lasers.

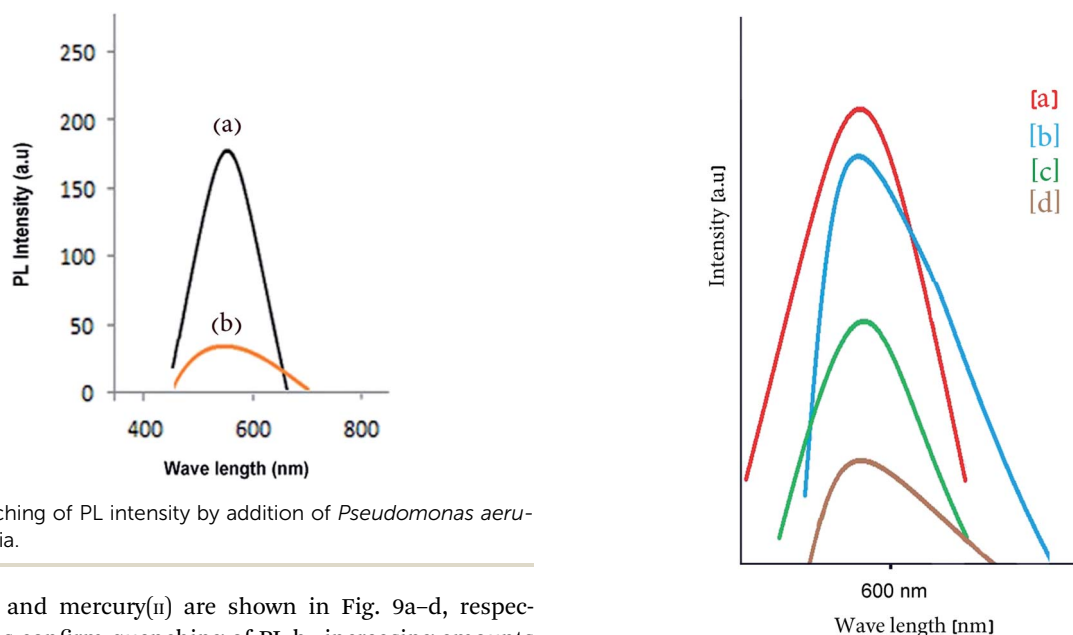


Fig. 8 Quenching of PL intensity by addition of *Pseudomonas aeruginosa* bacteria.

cadmium(II) and mercury(II) are shown in Fig. 9a–d, respectively. Results confirm quenching of PL by increasing amounts with Ni(II), Cd(II) and Hg(II) ions. The  $\text{MgFe}_2\text{O}_4$ -carbon nanostructure is thus a suitable sensor for detecting toxic heavy metals. d-Orbitals of metal(II) ions can accept excited electron from carbon dots. With the addition of ions, the fluorescence of the CDs is quenched because of the formation of complexes between ion(II) and CDs (electron transfer process).<sup>3</sup> PL spectra at various concentrations of CDs-labeled Cd(II) were analyzed so that concentration of these hazardous ions could be measured.<sup>1–4</sup>

Fig. 9 PL intensity of (a) pure carbon dots. Quenching by addition of toxic heavy-metal ions: (b) Ni(II), (c) Cd(II), (d) Hg(II).

## 4. Conclusion

Carbon dots have attracted much attention due to their rare electron excitation–relaxation properties. Photoluminescence nanostructures were attached to a  $\text{MgFe}_2\text{O}_4$  porous structure. Owing to pores in magnesium ferrite, carbon dots can diffuse to the inorganic Mg-ferrite core so we have simultaneously both





magnetism and luminescence. The nanocomposite is feasible for sensing of harmful bacteria in waste water, and with the help of the magnetic core it can easily be collected after use. *Pseudomonas aeruginosa* and toxic metal ions can be detected by applying fluorescent carbon nanostructures.

## Conflicts of interest

There are no conflicts to declare.

## Acknowledgements

Professor Masoud Salavati-Niasari and co-workers at the Institute of Nano Science and Nano Technology, University of Kashan, Iran are acknowledged for kindly providing access to the analysis facility. This work was funded by grant no. 159271/4AHM from University of Kashan and the council of Iran National Science Foundation (INSF, 97017837).

## References

- 1 S. Ahmadian-Fard-Fini, M. Salavati-Niasari and D. Ghanbari, Hydrothermal green synthesis of magnetic Fe<sub>3</sub>O<sub>4</sub>-carbon dots by lemon and grape fruit extracts and as a photoluminescence sensor for detecting of *E. coli* bacteria, *Spectrochim. Acta, Part A*, 2018, **203**, 481–493.
- 2 D. Bera, L. Qian, T. K. Tseng and P. H. Holloway, Quantum Dots and Their Multimodal Applications: A Review, *Materials*, 2010, **3**(4), 2260.
- 3 S. Ahmadian-Fard-Fini, D. Ghanbari and M. Salavati-Niasari, Photoluminescence carbon dot as a sensor for detecting of *Pseudomonas aeruginosa* bacteria: Hydrothermal synthesis of magnetic hollow NiFe<sub>2</sub>O<sub>4</sub>-carbon dots nanocomposite material, *Composites, Part B*, 2019, **161**, 564–577.
- 4 S. Ahmadian-Fard-Fini, D. Ghanbari, O. Amiri and M. Salavati-Niasari, Electro-spinning of cellulose acetate nanofibers/Fe/carbon dot as photoluminescence sensor for mercury (II) and lead (II) ions, *Carbohydr. Polym.*, 2020, **229**, 115428.
- 5 M. K. Barman and A. Patra, Current status and prospects on chemical structure driven photoluminescence behaviour of carbon dots, *J. Photochem. Photobiol., C*, 2018, **37**, 1–22.
- 6 R. Das, R. Bandyopadhyay and P. Pramanik, Carbon quantum dots from natural resource: A review, *MaterToday Chem*, 2018, **8**, 96–109.
- 7 L. Lin, Y. Luo, P. Tsai, J. Wang and X. Chen, Metal ions doped carbon quantum dots: Synthesis, physicochemical properties, and their applications, *TrAC, Trends Anal. Chem.*, 2018, **103**, 87–101.
- 8 P. Tian, L. Tang, K. S. Teng and S. P. Lau, Graphene quantum dots from chemistry to applications, *MaterToday Chemistry*, 2018, **10**, 221–258.
- 9 M. Abhilash, Quantitative structure activity relationship, *Int. J. Pharma Bio Sci.*, 2010, **V1**(1), 1.
- 10 A. Abbas, L. T. Mariana and A. N. Phan, Biomass-waste derived graphene quantum dots and their applications, *Carbon*, 2018, **140**, 77–99.
- 11 Y. W. Son, M. L. Cohen and S. G. Louie, Energy Gaps in Graphene Nanoribbons, *Phys. Rev. Lett.*, 2006, **97**, 216803.
- 12 S. Sharma, A. Umar, S. Sood, S. K. Mehta and S. K. Kansal, Photoluminescent C-dots: An overview on the recent development in the synthesis, physicochemical properties and potential applications, *J. Alloys Compd.*, 2018, **748**, 818–853.
- 13 R. Kumar, V. B. Kumar and A. Gedanken, Sonochemical synthesis of carbon dots, mechanism, effect of parameters, and catalytic, energy, biomedical and tissue engineering applications, *Ultrason. Sonochem.*, 2020, **64**, 105009.
- 14 K. Hedayati, D. Ghanbari, M. Kord and M. Goodarzi, (Co, Ag, Ni, Cd, Mn, Cr)-doped PbS photo-catalyst: sonochemical-assisted synthesis of magnetite nanocomposites applicable for elimination of toxic pollutants, *J. Mater. Sci.: Mater. Electron.*, 2021, **32**(1), 373–383.
- 15 R. J. Wood, J. Lee and M. J. Bussemaker, A parametric review of sonochemistry: Control and augmentation of sonochemical activity in aqueous solutions, *Ultrason. Sonochem.*, 2017, **38**, 351–370.
- 16 J. Yoo, H.-S. Kim, S.-Y. Park, S. Kwon, J. Lee, J. Koo and Y.-S. Seo, Instantaneous integration of magnetite nanoparticles on graphene oxide assisted by ultrasound for efficient heavy metal ion retrieval, *Ultrason. Sonochem.*, 2020, **64**, 104962.
- 17 K. Tian, F. Nie, K. Luo, X. Zheng and J. Zheng, A sensitive electrochemiluminescence glucose biosensor based on graphene quantum dot prepared from graphene oxide sheets and hydrogen peroxide, *J. Electroanal. Chem.*, 2017, **801**, 162–170.
- 18 S. Demirci, A. B. McNally, R. S. Ayyala, L. B. Lawson and N. Sahiner, Synthesis and characterization of nitrogen-doped carbon dots as fluorescent nanoprobe with antimicrobial properties and skin permeability, *J. Drug Delivery Sci. Technol.*, 2020, **59**, 101889.
- 19 T. Ge, Z. Jiang, L. hen, J. Li, Z. Lu, Y. Zhang and F. Wang, Synthesis and application of Fe<sub>3</sub>O<sub>4</sub>/FeWO<sub>4</sub> composite as an efficient and magnetically recoverable visible light-driven photocatalyst for the reduction of Cr(VI), *Sep. Purif. Technol.*, 2021, **263**, 118401.
- 20 Z. Jiang, K. Chen, Y. Zhang, Y. Wang, F. Wang, G. Zhang and D. D. Dionysiou, Magnetically recoverable MgFe<sub>2</sub>O<sub>4</sub>/conjugated polyvinyl chloride derivative nanocomposite with higher visible-light photocatalytic activity for treating Cr(VI)-polluted water, *Sep. Purif. Technol.*, 2020, **236**, 116272.
- 21 A. Balcht and R. Smith, *Pseudomonas aeruginosa: Infections and Treatment*, Informa Health Care, 1994, pp. 83–84, ISBN 0-8247-9210-6.
- 22 L. Yu, L. Zhang, G. Ren, S. Li, B. Zhu, F. Chai, F. Qu, C. Wang and Z. Su, Multicolorful fluorescent-nanoprobe composed of Au nanocluster and carbon dots for colorimetric and fluorescent sensing Hg<sup>2+</sup> and Cr<sup>6+</sup>, *Sens. Actuators, B*, 2018, **262**, 678–686.
- 23 N. Høiby, O. Ciofu and T. Bjarnsholt, *Pseudomonas aeruginosa* biofilms in cystic fibrosis, *Future Microbiol.*, 2010, **5**(11), 1663–1674.

